

VLT-FLAMES Analysis of 8 giants in the Bulge Metal-poor Globular Cluster NGC 6522: Oldest Cluster in the Galaxy? [★]

Analysis of 8 giants in NGC 6522

B. Barbuy¹, M. Zoccali², S. Ortolani³, V. Hill⁴, D. Minniti^{1,5}, E. Bica⁶, A. Renzini⁷, and A. Gómez⁴

- ¹ Universidade de São Paulo, IAG, Rua do Matão 1226, Cidade Universitária, São Paulo 05508-900, Brazil; e-mail: barbuy@astro.iag.usp.br
² Universidad Católica de Chile, Departamento de Astronomía y Astrofísica, Casilla 306, Santiago 22, Chile; e-mail: mzoccali@astro.puc.cl, dante@astro.puc.cl
³ Università di Padova, Dipartimento di Astronomia, Vicolo dell'Osservatorio 2, I-35122 Padova, Italy; e-mail: sergio.ortolani@unipd.it
⁴ Observatoire de Paris-Meudon, 92195 Meudon Cedex, France; e-mail: Vanessa.Hill@obspm.fr, anita.gomez@obspm.fr
⁵ Specola Vaticana, Vatican Observatory, V00120 Vatican City State, Italy
⁶ Universidade Federal do Rio Grande do Sul, Departamento de Astronomia, CP 15051, Porto Alegre 91501-970, Brazil; e-mail: bica@if.ufrgs.br
⁷ Osservatorio Astronomico di Padova, Vicolo dell'Osservatorio 5, I-35122 Padova, Italy; e-mail: alvio.renzini@oapd.inaf.it

Received; accepted

ABSTRACT

Context. NGC 6522 has been the first metal-poor globular cluster identified in the bulge by W. Baade. Despite its importance, very few high resolution abundance analyses of stars in this cluster are available in the literature. The bulge metal-poor clusters may be important tracers of the early chemical enrichment of the Galaxy.

Aims. The main purpose of this study is the determination of metallicity and elemental ratios in individual stars of NGC 6522.

Methods. High resolution spectra of 8 giants of the bulge globular cluster NGC 6522 were obtained at the 8m VLT UT2-Kueyen telescope with the FLAMES+GIRAFFE spectrograph. Multiband *V, I, J, K_s* photometry was used to derive effective temperatures as reference values. Spectroscopic parameters are derived from Fe I and Fe II lines, and adopted for the derivation of abundance ratios.

Results. The present analysis provides a metallicity $[Fe/H] = -1.0 \pm 0.2$. The α -elements Oxygen, Magnesium and Silicon show $[O/Fe]=+0.4\pm 0.3$, $[Mg/Fe]=[Si/Fe]= +0.25\pm 0.15$, whereas Calcium and Titanium show shallower ratios of $[Ca/Fe]=[Ti/Fe]=+0.15\pm 0.15$. The neutron-capture *r*-process element Europium appears to be overabundant by $[Eu/Fe]=+0.4\pm 0.4$. The neutron-capture *s*-elements La and Ba are enhanced by $[La/Fe]=+0.35\pm 0.2$ and $[Ba/Fe]=+0.5\pm 0.5$. The large internal errors, indicating the large star-to-star variation in the Ba and Eu abundances, are also discussed.

Conclusions. The moderate metallicity combined to a blue Horizontal Branch (BHB), are characteristics similar to those of HP 1 and NGC 6558, pointing to a population of very old globular clusters in the Galactic bulge. Also, the abundance ratios in NGC 6522 resemble those in HP 1 and NGC 6558. The ultimate conclusion is that the bulge is old, and went through an early prompt chemical enrichment.

Key words. Galaxy: Bulge - Globular Clusters: NGC 6522 - Stars: Abundances, Atmospheres

1. Introduction

Metal-poor bulge field stars and clusters represent a crucial piece in the puzzle of the Milky Way formation. NGC 6522 and its surrounding fields, located in the Large Sagittarius Cloud, were observed by Baade (1946), that identified part of the Cloud as a window reaching the nuclear bulge, since then called Baade's Window. Baade concluded, for the first

time, that its stellar population is of type II. Blanco & Blanco (1984) and Walker and Mack (1986) presented B,V data on NGC 6522, and the latter authors concluded that NGC 6522 is moderately metal-poor.

Lee (1992) has shown that the metallicity distribution of RR Lyrae variables in the Galactic bulge is more metal-rich than in the halo, with a peak metallicity at $[Fe/H]\approx -1.0$. This is interpreted as an age effect, given that more metal-rich stars are expected to populate the red horizontal branch (RHB), and only lower mass (and older) stars would be bluer falling in the RR Lyrae gap. This implies as well that the oldest stellar population of the Galaxy is found in the Galactic bulge.

Send offprint requests to: B. Barbuy

[★] Observations collected both at the European Southern Observatory, Paranal, Chile (ESO) programmes 71.B-0617A, 73.B0074A).

Lee et al. (2007) showed all clusters with extended blue horizontal branches (EHB) are the most massive and brightest globular clusters of the Milky Way, all of them brighter than magnitudes $M_V < -7$. NGC 6522 is classified as having a moderately extended EHB and estimated integral magnitude of $M_V = -7.67$ (Harris, 1996, updated in www.physics.mcmaster.ca/Globular.html), or -7.99 (Armandroff 1989), and is therefore at the edge of the distribution of massive clusters. Lee et al. (2007) suggested that NGC 6522 is among relics of the first building blocks that first assembled to form the Galactic nucleus, and that are now observed as relatively metal-poor EHB globular clusters.

Therefore, NGC 6522, together with other bulge clusters such as HP 1 (Barbuy et al. 2006a) and NGC 6558 (Barbuy et al. 2007), could be relics of primeval star-forming sub-systems that first formed the Galactic center population. This could have been achieved both by dissipational and dissipationless mergers, as has been predicted by recent Λ CDM simulations of high- σ peaks (e.g. Diemand et al. 2005; Moore et al. 2006).

The globular cluster NGC 6522, also designated GCl 82, C 1800-300 and Cl VDBH 256, is located at J2000 $\alpha = 18^{\text{h}}03^{\text{m}}34.08^{\text{s}}$, $\delta = -30^{\circ}02'02.3''$, and projected at 4° from the Galactic center ($l=1.0246^{\circ}$, $b=-3.9256^{\circ}$). It is at a distance $d_{\odot} = 6$ kpc away from the Sun, and at $R_{\text{GC}} = 2$ kpc from the Galactic center (Barbuy et al. 1998).

Terndrup et al. (1998) derived proper motions of $\langle\mu_l\rangle = 1.4 \pm 0.2$ mas yr $^{-1}$, $\langle\mu_b\rangle = -6.2 \pm 0.2$ mas yr $^{-1}$, and a mean radial velocity of $v_r = -28.5 \pm 6.5$ km s $^{-1}$, and concluded that the cluster stays in the bulge.

Literature basic parameters of NGC 6522 are gathered in Table 1. Minniti et al. (1995) presented a first K vs. J-K Colour-Magnitude Diagram (CMD) of NGC 6522. The cluster has a concentration parameter $c=2.50$, a core radius $\log r_c(') = 0.49$, and a half-light radius of $\log r_h(') = 1.78$ (Trager et al. 1995).

Among the metal-poor clusters of the inner bulge, Terzan 4 ($[\text{Fe}/\text{H}]=-1.6$) has been studied with high resolution infrared spectroscopy (Origlia & Rich 2004), revealing significant enhancement of the α -elements. HP 1 ($[\text{Fe}/\text{H}]=-1.0$) and NGC 6558 ($[\text{Fe}/\text{H}]=-1.0$) were studied with high resolution spectroscopy in the optical (Barbuy et al. 2006a, 2007), showing shallow α -element enhancements.

In this work we present a detailed abundance analysis of 8 stars in NGC 6522, based on high resolution spectra obtained with FLAMES+GIRAFFE at the ESO Very Large Telescope VLT-UT2 Kueyen, at Paranal. The detailed analysis is carried out using updated MARCS model atmospheres (Gustafsson et al. 2008).

The observations are described in Sect. 2. Photometric stellar parameters effective temperature and gravity are derived in Sect. 3. Atomic and molecular data are reviewed in Sect. 4. Spectroscopic parameters are derived in Section 5 and abundance ratios are computed in Sect. 6. A discussion is presented in Sect. 7 and conclusions are drawn in Sect. 8.

Table 1. Parameters of NGC 6522 given in the literature. References: 1 Zinn 1985; 2 Armandroff 1989; 3 Harris 1996; 4 Rutledge et al. 1997a; 5 Rutledge et al. 1997b (given in Zinn & West 1984 and Carretta & Gratton metallicity scales); 6 Terndrup & Walker 1994; 7 Terndrup et al. 1998 ($A_V=1.42$ is given); 8 Piotto et al. 2002; 9 Kraft & Ivans 2003; 10 Bica et al. 2006.

E(B-V)	[Fe/H]	v_r (km s $^{-1}$)	$(m - M)$	d_{\odot} (kpc)	ref.
0.45	-1.44	+8	15.37	6.2	1
—	-1.44	-3	—	—	2
0.48	-1.44	-21.1	16.52	7.8	3
0.50	-1.44	-18.7	—	—	4
—	-1.50/-1.21	—	—	—	5
0.52	-1.60	—	—	—	6
0.39	-1.28	-28.5	—	7.3	7
0.48	-1.44	—	—	7.4	8
—	-1.44/-1.42/-1.35	—	—	—	9
0.48	-1.44	—	—	7.8	10

2. The Data

2.1. Imaging

V and I data of NGC 6522 and surrounding fields were collected from the Optical Gravitational Lensing Experiment (OGLE) survey (Udalski et al. 1992, 1993). Target stars were cross identified in the 2MASS Point Source Catalogue (Skrutskie et al. 2006¹) and their J, H, and K_s magnitudes were used, except for the fainter sample stars B-108, B-122, B-130, F-121, for which no satisfactory identification in 2MASS data was found, their magnitudes being probably at the photometric limits of the 2MASS survey.

The location of target stars on the OGLE CMD is shown in Fig. 1. Six of the target stars were identified in the field of an ACS (Advanced Camera for Surveys) image retrieved from the archives of the Hubble Space Telescope, as shown in Fig. 2.

The selected stars, their coordinates, magnitudes and colours as obtained from the OGLE catalogue, together with the 2MASS designations (Skrutskie et al. 2006), coordinates and VIJHK_s magnitudes, are listed in Table 2. The star IDs are adopted according to the fact that FLAMES+GIRAFFE has provided spectra for 134 stars in each of the bright (B) and faint (F) stars selected in this field. The cluster members turned out to be star B8 (i.e., the 8th spectrum of the bright sample), and so forth, and such designations were kept.

2.2. Spectra

Spectra for about 200 giants in Baade's Window were obtained with FLAMES+GIRAFFE at the Very Large Telescope, within our large program for a spectroscopic characterization of bulge field stars (Zoccali et al. 2006, 2008; Lecureur et al. 2007). The

¹ <http://ipac.caltech.edu/2mass/releases/allsky/>

Table 2. Identifications, positions, magnitudes, and dereddened colours adopting the reddening law by Dean et al. (1978) and Rieke & Lebofsky (1985).

star	2MASS ID	α_{2000}	δ_{2000}	V	I	J	H	K_s	K_{TCS}	$V-I_{J_0}$	$V-K_{TCS_0}$	$J-K_{TCS_0}$
B-008	18034605-3000512	18:03:46.04	-30:00:50.9	15.99	14.384	13.099	12.336	12.198	12.205	1.008	2.548	0.626
B-107	18033660-3002164	18:03:36.59	-30:02:16.1	15.98	14.316	13.006	11.803	11.574	12.008	1.066	2.735	0.726
B-108	—	18:03:35.18	-30:02:04.9	16.29	14.403	—	—	—	—	1.289	—	—
B-118	18034225-3003403	18:03:42.24	-30:03:39.9	16.01	14.309	13.056	12.305	12.142	12.149	1.103	2.624	0.638
B-122	—	18:03:33.34	-30:01:58.3	16.00	14.280	—	—	—	—	1.122	—	—
B-128	18034463-3002107	18:03:44.61	-30:02:10.4	16.26	14.553	12.860	12.614	12.438	12.442	1.109	2.578	0.166
B-130	—	18:03:41.00	-30:03:03.0	16.30	14.640	—	—	—	—	1.062	—	—
B-134	18034117-3002218	18:03:41.16	-30:02:21.6	16.04	14.493	13.286	12.768	12.563	12.569	0.949	2.233	0.455
F-121	18033640-3002221	18:03:36.41	-30:02:19.8	16.40	14.676	12.586	12.065	11.729	11.584	1.126	3.580	1.135

Table 3. Log of the spectroscopic observations carried out on 2003 May 7 (Julian Date 2452766), 2003 June 7, 11, 23, 26 (Julian Dates 2452797, 2452801, 2452813, 2452816) and 2003 July 20 (Julian Date 2452840). Slit widths of 0.8" and 1.0" were used, depending on the seeing value. The quoted seeing is the mean value along the exposures.

Target	setup	date	UT	exp (s)	Airmass	Seeing (")	(S/N)/px	v_r^{obs} kms ⁻¹	Mean kms ⁻¹	$v_r^{\text{hel.}}$ kms ⁻¹	Mean kms ⁻¹
B-008	HR13	07.05.03	05:37:22.3	5400	1.15	0.96"	128	-30.088	-29.5	-9.03	-19.8
	HR14	23.06.03	03:50:00.5	9900	1.025	0.68"	107	-28.762		-28.82	
	HR15	07.06.03	03:49:11.9	3600	1.115	0.57"	160	-29.633		-21.52	
B-107	HR13	07.05.03	05:37:22.3	5400	1.15	0.96"	120	-27.633	-27.3	-6.59	-17.7
	HR14	23.06.03	03:50:00.5	9900	1.025	0.68"	120	-26.527		-26.60	
	HR15	07.06.03	03:49:11.9	5400	1.15	0.96"	194	-27.751		-19.94	
B-108	HR13	07.05.03	05:37:22.3	5400	1.15	0.96"	110	-33.111	-32.7	-12.07	-23.0
	HR14	23.06.03	03:50:00.5	9900	1.025	0.68"	106	-33.605		-33.60	
	HR15	07.06.03	03:49:11.9	5400	1.15	0.96"	100	-31.244		-23.44	
B-118	HR13	07.05.03	05:37:22.3	5400	1.15	0.96"	94	-43.045	-41.7	-22.00	-32.0
	HR14	23.06.03	03:50:00.5	9900	1.025	0.68"	92	-42.293		-42.35	
	HR15	07.06.03	03:49:11.9	5400	1.15	0.96"	92	-39.806		-31.99	
B-122	HR13	07.05.03	05:37:22.3	5400	1.15	0.96"	85	-36.900	-36.1	-15.86	-26.9
	HR14	23.06.03	03:50:00.5	9900	1.025	0.68"	99	-35.765		-36.87	
	HR15	07.06.03	03:49:11.9	5400	1.15	0.96"	114	-35.640		-27.83	
B-128	HR13	07.05.03	05:37:22.3	5400	1.15	0.96"	90	-33.331	-32.7	-12.28	-23.1
	HR14	23.06.03	03:50:00.5	9900	1.025	0.68"	105	-32.982		-33.04	
	HR15	07.06.03	03:49:11.9	5400	1.15	0.96"	106	-31.866		-24.04	
B-130	HR13	07.05.03	05:37:22.3	5400	1.15	0.96"	78	-36.713	-34.9	-15.67	-25.3
	HR14	23.06.03	03:50:00.5	9900	1.025	0.68"	96	-34.756		-34.82	
	HR15	07.06.03	03:49:11.9	5400	1.15	0.96"	108	-33.225		-25.41	
B-134	HR13	07.05.03	05:37:22.3	5400	1.15	0.96"	122	-39.272	-37.8	-18.22	-28.2
	HR14	23.06.03	03:50:00.5	9900	1.025	0.68"	103	-38.512		-38.57	
	HR15	07.06.03	03:49:11.9	5400	1.15	0.96"	123	-35.634		-27.81	
F-121	HR13	11.06.03	08:46:34.2	8100	1.39	0.36"	92	-29.813	-29.2	-24.48	-28.0
	HR14	20.07.03	02:25:59.6	16500	1.01	1.03"	83	-29.373		-29.37	
	HR15	26.06.03	05:50:32.3	6000	1.06	0.69-0.86"	98	-28.467		-30.27	

four fields of this survey include a few bulge globular clusters, and some fibres were positioned close to their centers in order to determine consistent abundances for bulge field and cluster stars. Having measured the radial velocity of the 200 spectra in this field, candidate cluster members were identified by select-

ing stars with radial velocities and coordinates within a radius of 2.7 arcmin from the cluster center, therefore within the core radius. Nine candidates were then identified, eight of which turned out to have very similar metallicity (lower than the bulk of bulge stars) and hence appeared to belong to NGC 6522.

Table 4. Photometric stellar parameters derived using the calibrations by Alonso et al. (1999) for $V - I$, $V - K$, $J - K$, bolometric corrections, bolometric magnitudes and corresponding gravity $\log g$, and final spectroscopic parameters.

star	Photometric parameters						Spectroscopic parameters					
	$T(V - I)$ K	$T(V - K)$ K	$T(J - K_{\text{TCS}})$ K	BC_V	M_{bol}	$\log g$	T_{eff} K	$\log g$	[FeI/H]	[FeII/H]	[Fe/H]	v_t km s ⁻¹
B-008	4867	4615	4597	-0.32	0.93	2.52	4600	2.0	-1.00	-1.06	-1.03	1.40
B-107	4745	4465	4311	-0.37	0.97	2.50	4900	2.1	-1.15	-1.06	-1.11	1.40
B-108	4349	—	—	-0.58	1.50	2.55	4700	2.6	-1.12	-1.08	-1.10	0.80
B-118	4671	4552	4558	-0.40	1.03	2.49	4700	2.6	-0.87	-0.81	-0.84	1.30
B-122	4635	—	—	-0.41	1.04	2.48	4800	2.6	-0.87	-0.87	-0.87	1.10
B-128	4660	4589	6914	-0.40	1.28	2.58	4800	2.7	-0.79	-0.79	-0.79	1.30
B-130	4753	—	—	-0.36	1.28	2.62	4800	2.3	-1.09	-1.10	-1.09	1.40
B-134	5000	4912	5212	-0.28	0.94	2.57	—	—	—	—	—	—
F-121	4627	—	—	-0.42	1.44	2.64	4750	2.3	-1.14	-1.15	-1.15	1.30

High resolution spectra of 9 stars in NGC 6522, in the wavelength range $\lambda\lambda$ 6100-6860 Å, were obtained through the GIRAFFE setups HR13 ($\lambda\lambda$ 6120-6402 Å), HR14 ($\lambda\lambda$ 6381-6620 Å) and HR15 ($\lambda\lambda$ 6605-6859 Å), at a resolution $R=22,000$. Log of observations are given in Table 3. The spectra were flatfielded, optimally-extracted and wavelength calibrated with the GIRAFFE Base-Line Data Reduction Software pipeline (girBLDRS²). Spectra extracted from different frames were then summed, and the final spectra of ~ 15 fibres positioned on empty sky regions were further combined together and subtracted from each star spectrum. S/N ratio were measured in the co-added spectra, at several wavelength regions encompassing around 2 to 3 Å, from 6200 to 6500 Å, and the values reported in Table 3 are the mean of these measurements. No clear continuum window could be identified in the spectra from the HR15 setup, hence S/N values were not measured in this region. The equivalent widths were measured using the automatic code DAOSPEC, developed by Stetson & Pancino (2008). The stars B-108 and B-134 presented problems to converge in terms of spectroscopic parameters, and a check line by line was needed in order to eliminate from the list any lines showing blends or cosmic ray hits. A check on zoomed parts of the ACS image (Fig. 2), given in Figs. 3, shows that B-108 is near the cluster center, therefore in a very crowded region, where contamination could be possible, whereas B-134 has a fainter companion, having a probable contamination of lines. B-134 was finally discarded from the sample, due to a clear contamination of its spectrum.

A radial velocity $v_r = -33.5 \pm 0.7$ km s⁻¹ or heliocentric radial velocity $v_r^{\text{hel}} = -24.9 \pm 0.7$ km s⁻¹ was found for NGC 6522, in good agreement with values of $v_r^{\text{hel}} = -18.3 \pm 9.3$ km s⁻¹ by Rutledge et al. (1997a,b), $v_r^{\text{hel}} = -28.5 \pm 6.5$ km s⁻¹ derived by Terndrup et al. (1998), and the value of $v_r^{\text{hel}} = -21.1 \pm 3.4$ reported in the compilation by Harris (1996).

3. Stellar Parameters

3.1. Temperatures

Terndrup & Walker (1994) obtained BVI photometry on several fields of Baade's Window and NGC 6522. Fits to CMDs relative to other globular clusters having the same Red Giant Branch (RGB) morphology, resulted in $E(B-V)=0.52$ for $B-V=0$ stars, corresponding to about 0.44-0.45 for our K and M stars. Terndrup et al. (1998) derived $A_V=1.4$ on a proper motion cleaned CMD of NGC 6522. This gives again about $E(B-V)=0.45$ for K and M stars. We conclude that NGC 6522 has a reddening close to 0.44-0.45, compatible with other authors (see Table 1). For the present analysis we adopt the extinction law given by Dean et al. (1978) and Rieke & Lebofsky (1985), namely, $R_V = A_V/E(B-V) = 3.1$, $E(V-I)/E(B-V)=1.33$, $E(V-K)/E(B-V)=2.744$, $E(J-K)/E(B-V)=0.527$, implying in colour corrections of $A_I/E(B-V) = 1.77$; $A_J/E(B-V) = 0.88$, $A_H/E(B-V) = 0.55$; $A_K/E(B-V) = 0.356$.

Effective temperatures were derived from $V - K$, $V - I$ and $J - K$ using the colour-temperature calibrations of Alonso et al. (1999, hereafter AAM99), and using $(V - I)_C=0.778(V - I)_J$ (Bessell 1979). The J, H, K_S magnitudes and colours were transformed from the 2MASS system to CIT (California Institute of Technology), and from this to TCS (Telescopio Carlos Sánchez), using the relations established by Carpenter (2001) and Alonso et al. (1998). As mentioned above, no JHK_S magnitudes are given for B-108, B-122, B-130, F-121.

The derived photometric effective temperatures are listed in Table 4.

3.2. Gravities

The classical relation:

$$\log g_* = 4.44 + 4 \log \frac{T_*}{T_\odot} + 0.4(M_{\text{bol}} - 4.75) + \log \frac{M_*}{M_\odot}$$

was used, adopting $T_\odot=5770$ K, $M_*=0.85 M_\odot$ and $M_{\text{bol}\odot} = 4.75$.

² <http://girbldrs.sourceforge.net>

A distance modulus of $(m-M)_0 = 13.91$ together with a total extinction $A_V = 1.72$ were adopted (Barbuy et al. 1998). The bolometric corrections from AAM99 and corresponding gravities are given in Table 4.

4. Atomic and molecular data

The Fe I line list and respective oscillator strengths used were described in Zoccali et al. (2004), Barbuy et al. (2006a, 2007), and reported in Table A.1, where they are compared with values given in the NIST database (Fuhr & Wiese 2006). Five measurable Fe II lines, and their respective oscillator strengths from Biémont et al. (1991), and renormalized by Meléndez & Barbuy (2009), were used to check whether ionization equilibrium was verified.

In Barbuy et al. (2006a) the damping constants and gf -values selected in Zoccali et al. (2004) were revised concerning NaI, MgI, SiI, CaI, TiI and TiII lines. The damping constants for all lines had been computed where possible, and in particular for most of the Fe I lines, using the collisional broadening theory of Barklem et al. (1998, 2000 and references therein). For NaI, MgI, SiI, CaI, TiI and TiII lines we adopted a mean of $\gamma(\text{Barklem})/\gamma(\text{best fit}) \approx 1.5$ (cf. Barbuy et al. 2006a). The adopted oscillator strengths $\log gf$ and interaction constants C_6 are given in Table 7.

For the forbidden oxygen line [OI]6300 Å we adopt the oscillator strength derived by Allende Prieto et al. (2001): $\log gf = -9.716$. For lines of the heavy elements BaII, LaII and EuII, a hyperfine structure was taken into account, based on the hyperfine constants and splittings by Lawler et al. (2001a) for EuII 6645 Å, Lawler et al. (2001b) for LaII 6390 Å and McWilliam (1998) for BaII 6141 and constants and central wavelength from Rutten (1978), and hyperfine structure computed employing code made available by A. McWilliam for BaII 6496 Å. Solar isotopic ratios, and total $\log gf$ values from Hill et al. (2002), Lawler et al. (2001b) and Rutten (1978) were adopted, as indicated in Table 7. Molecular lines of CN ($A^2\Pi-X^2\Sigma$), C_2 Swan ($A^3\Pi-X^3\Pi$), TiO ($A^3\Phi-X^3\Delta$) γ and TiO ($B^3\Pi-X^3\Delta$) γ' systems are taken into account. Solar abundances were adopted from Grevesse & Sauval (1998), except for oxygen where $\epsilon(\text{O}) = 8.77$ was assumed, as recommended by Allende Prieto et al. (2001) for the use of 1-D model atmospheres.

5. Iron abundances

Photospheric 1-D models for the sample giants were extracted from the new MARCS model atmospheres grid (Gustafsson et al. 2008). The LTE abundance analysis and the spectrum synthesis calculations were performed using the code described in Cayrel et al. (1991), Barbuy et al. (2003) and Coelho et al. (2005). An Iron abundance of $\epsilon(\text{Fe})=7.50$ (Grevesse & Sauval 1998) was adopted.

The line list of Fe I and Fe II lines was used in the derivation of stellar parameters, where lines with equivalent widths $20 < \text{EW} < 130$ mÅ were not considered. The line list of Fe lines, together with measured equivalent widths is given in Table A.1.

The stellar parameters were derived by initially adopting the photometric effective temperature and gravity, and then fur-

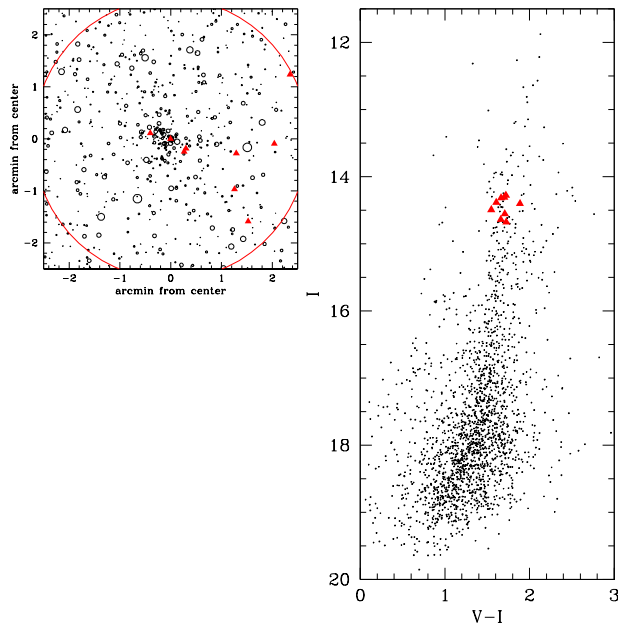


Fig. 1. OGLE Colour Magnitude Diagram of Baade's Window, with the sample stars of NGC 6522 overplotted.

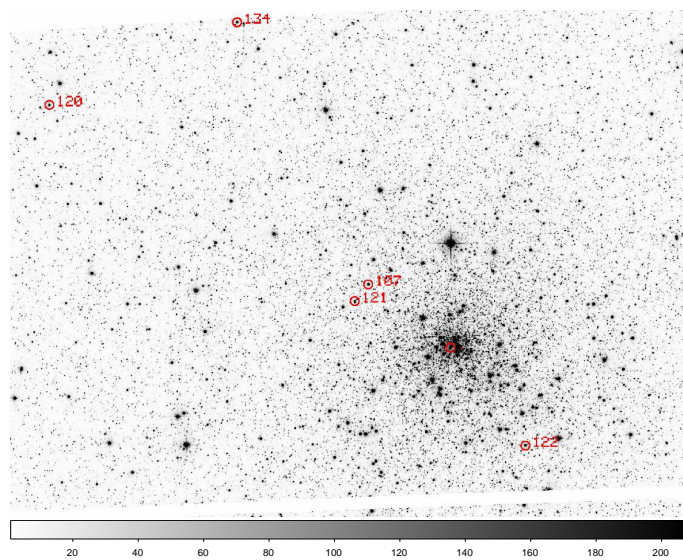


Fig. 2. ACS image of central parts of NGC 6522.

ther constraining the temperature by imposing excitation equilibrium for Fe I lines. Five Fe II lines were measurable, allowing to derive gravities imposing agreement between Fe I and Fe II abundances (ionization equilibrium). Microturbulence velocities v_t were determined by canceling the trend of Fe I abundance vs. equivalent width, using predicted EWs, as explained in Zoccali et al. (2008). The analysis uses the same procedures described in Zoccali et al. (2008) for the full sample of 800 bulge giants, with the differences that for NGC 6522 we use the known distance and reddening values, and the ionization equilibrium between Fe I and Fe II to derive gravities (whereas photometric gravities were adopted in Zoccali et al. 2008).

The final spectroscopic parameters T_{eff} , $\log g$, $[\text{Fe I}/\text{H}]$, $[\text{Fe II}/\text{H}]$, $[\text{Fe}/\text{H}]$ and v_t values are reported in the last columns of Table 4 and they were adopted for the derivation of abundance ratios. It is important to note that the newly revised oscillator strengths presented in Meléndez & Barbuy (2009), for Fe II lines, render both the gravities and the metallicities higher than would be derived with previous sets of $\log gf$ values.

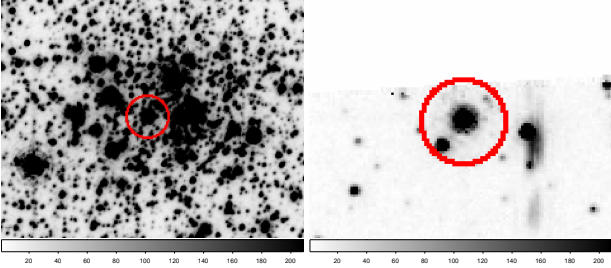


Fig. 3. Zoom of ACS image in the regions of B-108 and B-134. B-108 is located near the center of NGC 6522, and B-134 has a fainter companion. The image of B-134 is at the border of the ACS image.

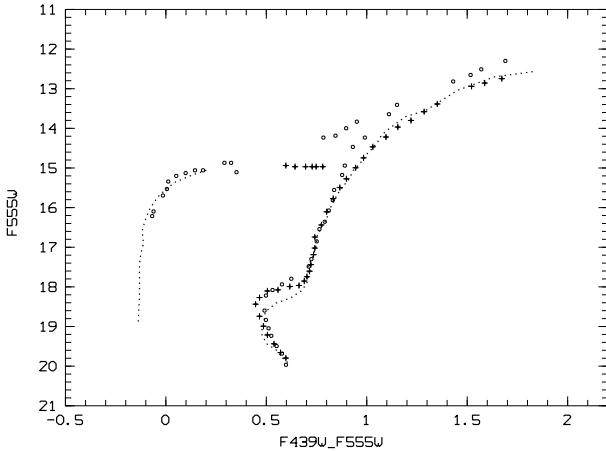


Fig. 4. Mean locus in V vs. V-I CMD of NGC 6522 (dots) compared to M5 (open circles) of $[\text{Fe}/\text{H}]=-1.2$, and 47 Tuc (crosses) of $[\text{Fe}/\text{H}]=-0.7$, based on HST-WFPC2 data from Piotto et al. (2002).

5.1. Errors

The errors within the spectroscopic parameter determination are given in Table 5, applied to the sample star NGC 6522: B-128. The error on the slope in the Fe I vs. ionization potential implies an error in the temperature of ± 100 K for the sample stars. An uncertainty of the order of 0.2 km s^{-1} on the microturbulence velocity is estimated from the imposition of constant value of $[\text{Fe}/\text{H}]$ as a function of EWs. Errors are given on Fe I and Fe II abundances, and other element abundance ratios, induced by a change of $\Delta T_{\text{eff}}=+100$ K, $\Delta \log g = +0.2$, $\Delta v_t = 0.2 \text{ km s}^{-1}$, and total error is given in the last column

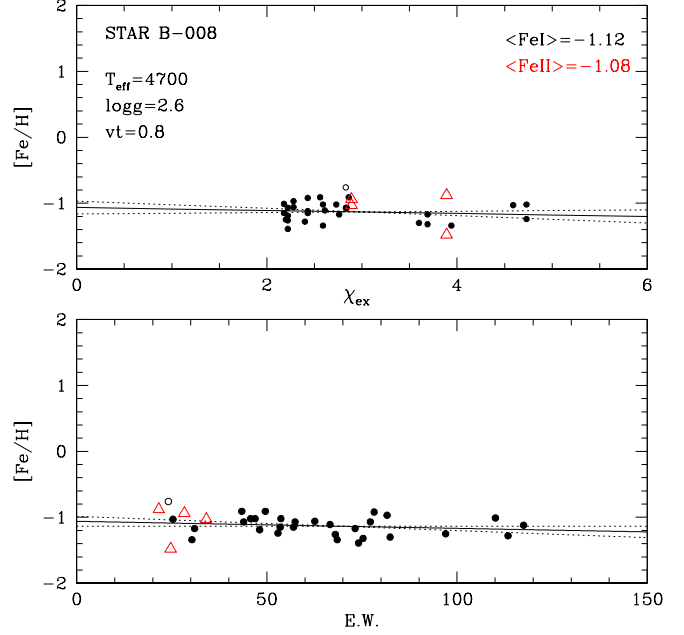


Fig. 5. Fe I and Fe II abundances vs. χ_{exc} (eV) and W_λ (mÅ) for star NGC 6522: B-8.

of Table 5. The errors indicated are to be added to the Fe I, Fe II abundances and abundance ratios derived in this work. It is also important to make clear that the errors in Fe I and Fe II abundances are not propagated into the abundance ratios.

Table 5. Abundance uncertainties for a $\Delta T_{\text{eff}} = 100$ K, $\Delta \log g = 0.2$, $\Delta v_t = 0.2 \text{ km s}^{-1}$ and corresponding total error. The errors are to be added to the reported abundances. The values given are a mean derived from the errors from each line.

Abundance	ΔT (100 K)	$\Delta \log g$ (+ 0.2 dex)	Δv_t (+ 0.2 km s^{-1})	$(\sum x^2)^{1/2}$
(1)	(2)	(3)	(4)	(5)
NGC6522 – B – 128				
[Fe I/H]	+0.06	0.00	-0.08	0.10
[Fe II/H]	-0.07	+0.11	-0.07	0.14
[O/Fe]	+0.08	0.00	+0.02	0.08
[Na I/Fe]	0.00	+0.05	0.00	0.05
[Mg I/Fe]	+0.05	+0.01	0.00	0.05
[Si I/Fe]	+0.15	0.00	0.00	0.15
[Ca I/Fe]	-0.03	+0.04	+0.05	0.07
[Ti I/Fe]	-0.08	0.00	+0.05	0.09
[Ti II/Fe]	0.00	-0.05	-0.01	0.05
[Ba II/Fe]	-0.02	+0.01	+0.15	0.15
[La II/Fe]	0.00	-0.10	0.00	0.10
[Eu II/Fe]	0.00	-0.20	0.00	0.20

6. Abundance ratios

Abundances ratios were obtained by means of line-by-line spectrum synthesis calculations compared to the observed lines, for the line list given in Table 7.

The fits to the NaI 6154.23 and SiII 6155.14 Å lines in Fig. 6a, CaI 6439.08 Å in Fig. 6b, and TiII 6559.576 Å in Fig. 6c for star B-8, illustrate the good quality of fits.

The odd-Z element sodium, built up during carbon burning, shows a solar ratio: $[Na/Fe] \sim 0.0$. The α -elements O, Mg and Si are enhanced by: $[O/Fe]=+0.39$, $[Mg/Fe]=+0.27$, $[Si/Fe]=+0.25$, whereas Ca and Ti show lower enhancements of $[Ca/Fe]=+0.17$ and $[Ti/Fe]=+0.16$. The r-process element Eu is enhanced by $[Eu/Fe]=+0.39$. The s-element La and Ba are enhanced with $[La/Fe]=0.35$ and $[Ba/Fe]=+0.49$, which is unexpected. For Ba there is also a star-to-star variation, and these issues are discussed below.

7. Discussion

We derived a metallicity of $[Fe/H]=-1.0 \pm 0.2$, and the element abundances reported in Tables 7 and 8, for 8 giants in the globular cluster NGC 6522.

7.1. Bulge globular clusters

In order to better characterize NGC 6522, in Table 6 we report globular clusters within $6^\circ \times 6^\circ$ of the Galactic center, classified by metallicity, and HB morphology. We identify a group of BHB clusters combined to a moderate metallicity of $[Fe/H] \sim -1.0$. As discussed in Barbuy et al. (2006a, 2007) regarding HP 1 and NGC 6558, these clusters should be very old (Lee et al. 1994). In this inner sample there are 6 over 19 objects in this class of globular clusters, and they constitute therefore a fraction around 30%. The last item in Table 6 concerns globular clusters that show similar properties to NGC 6522, i.e., a BHB and having moderate metallicity, that are located between 6° and 12° around the Galactic center; in this ring this class of clusters corresponds to a lower fraction of 16% of clusters, considerably lower with respect to the 30% fraction in the inner $6^\circ \times 6^\circ$ region, and we thus infer that this population appears to be more concentrated towards the Galaxy center.

As concerns the presence of RR Lyrae in the metal-poor inner bulge globular clusters, in particular those studied by means of spectroscopy so far (HP 1, NGC 6522, NGC 6558 and Terzan 4), from the most recent RR Lyrae compilation sources (Suntzeff et al. 1991, and the on-line catalogue published by Clement et al. (2001)³, the following can be extracted: there are no identified RR Lyrae stars in very metal-poor clusters Terzan 4, Terzan 9, and the moderately metal-poor NGC 6540. No studies on the recently discovered AL3 (Ortolani et al. 2006) are available. For HP1 there are 15 variable stars reported by Terzan (1964a,b, 1965, 1966) but none has been indicated as RR Lyrae. NGC 6558 has 9 confirmed RR Lyrae stars (Hazen 1996).

The field of NGC 6522 is very rich in RR Lyrae stars and they appear to be enhanced towards the center of the cluster.

Seven variables have been detected within $2'$ from the center of NGC 6522, but their membership is uncertain (Walker & Mack 1986; Clement et al. 1991). However Walker and Terndrup (1991), from radial velocities and metallicities, concluded that 4 of them should be RR Lyrae stars members of the cluster. From the DS index they obtained an average of $[Fe/H] \sim -1.0$, very near to the mean of the other Baade Window RR Lyrae stars they studied with the same method, but it is considered that the membership of these RR Lyrae stars to NGC 6522 remains an open issue.

As a conclusion, we suggest that the $[Fe/H] \sim -1.0$ RR Lyrae and our sample clusters of $[Fe/H] \sim -1.0$ and BHB, such as NGC 6522, could belong to the same stellar population.

7.2. Age of NGC 6522

In Fig. 4 we show the mean locus of NGC 6522 from Piotto et al. (2002) using Hubble Space Telescope F439W and F555W bands of the WFPC2 camera. Overplotted are the mean loci of M5 (NGC 5904) of $[Fe/H] = -1.2$ (e.g. Yong et al. 2008) and 47 Tuc of $[Fe/H] = -0.7$ (Alves-Brito et al. 2005), or -0.76 (Koch & McWilliam 2008). The RGB of NGC 6522 is very close to that of 47 Tuc, the latter slightly more metal-rich, and M5 is steeper. This confirms the metallicity higher than usually assigned to NGC 6522 (see Table 1). These high metallicities combined to a blue HB are not expected, and might have led to the lower metallicity estimates in the past.

Fig. 4 shows that the turnoff of NGC 6522 appears to be about 0.2 magnitudes fainter than those of 47 Tuc and M5, when the HBs are superimposed. This indicates an age about 2 Gyr older for NGC 6522. The older age is in agreement with the HB morphology because it is very blue for its relatively high metallicity.

In order to check this age difference between 47 Tuc and NGC 6522, in Fig. 8 we collected data from Piotto et al. (2002) for these two clusters, with colours transformed to B and V, and derived mean loci. Isochrones from Girardi et al. (2000) are then overplotted to these mean loci CMDs. For 47 Tuc, a metallicity of $Z=0.004$ ($[Fe/H] -0.7$) is adopted, with ages of 14.0 and 17.7 Gyr. It is clear that the 14 Gyr isochrone fits the data whereas this is not the case with 17.7 Gyr; for NGC 6522 the oldest isochrones of 17.7 Gyr for metallicities of $Z=0.004$ and 0.001 are overplotted. It is clear that this very old age fits the observed CMD with both metallicities. We also used α -enhanced Teramo isochrones from Pietrinferni et al. (2004), as described in the BASTI 2006 grid of models⁴, shown in Figs. 9. Adopting for 47 Tuc a metallicity of $Z=0.004$ ($[Fe/H] -0.7$), and ages of 11.0 and 14.0 Gyr, where the 11.0 Gyr one fits its CMD; and for NGC 6522 isochrones of 14.0 and 16.0 Gyr for a metallicity of $Z=0.002$ are overplotted. In this case the old age of 14.0 Gyr fits the observed CMD. This makes evident the old age of NGC 6522, although of course it cannot be older than 13.7 Gyr (Spergel et al. 2003), but the important result is its relative older age as compared with 47 Tuc.

Still, another way to estimate the age, despite more imprecise, is the HB parameter by Lee (1992) $(B-R)/(B+V+R)$,

³ <http://www.astro.utoronto.ca/~cclement/read.html>

⁴ <http://193.204.1.602/index.html>

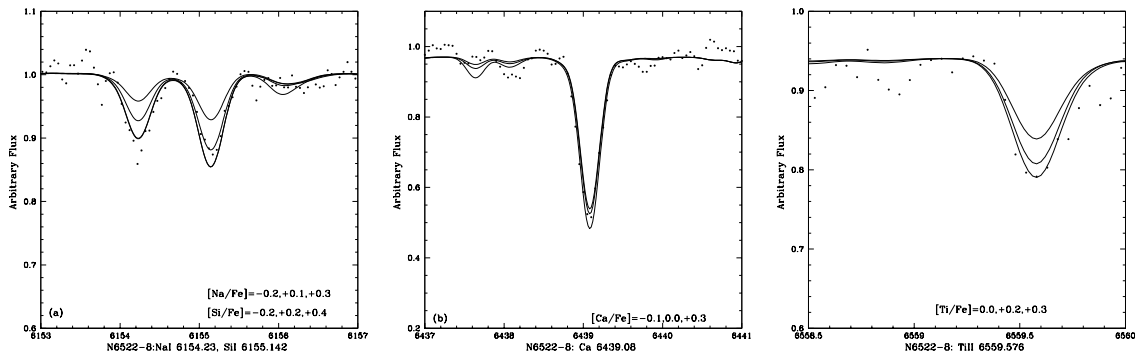


Fig. 6. Star B-8: (a) NaI 6154.230 and SiI 6155.142 Å fits. Faint dotted line is the observed spectrum. Solid lines show the computed spectra with abundance ratios $[Na/Fe] = -0.2, +0.1, +0.3$, and $[Si/Fe] = -0.2, +0.2, +0.4$; (b) Ca 6439.08 Å computed with $[Ca/Fe] = -0.1, 0.0, +0.3$; (c) TiII 6559.576 Å computed with $[Ti/Fe] = 0.0, +0.2, +0.3$.

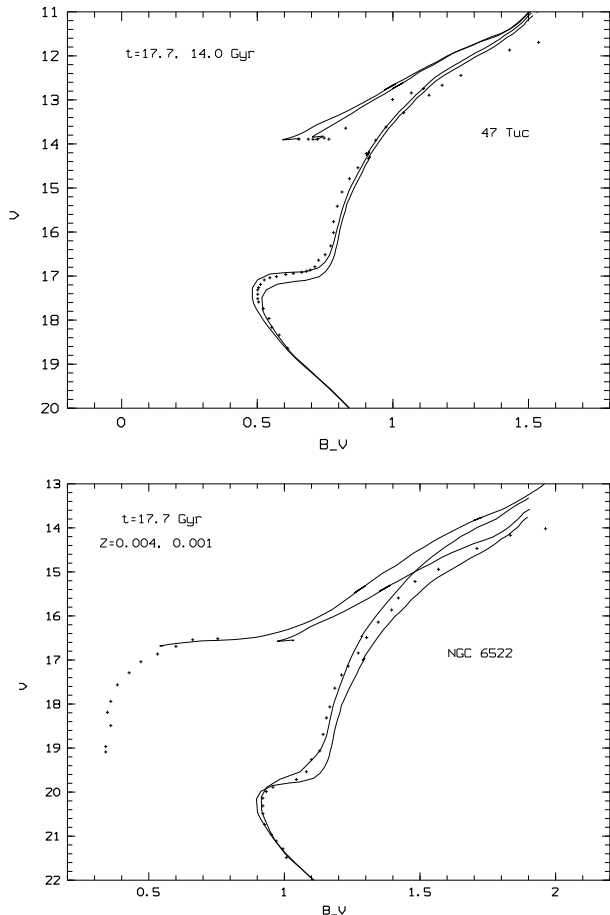


Fig. 8. Mean loci CMDs of 47 Tuc and NGC 6522, based on HST data from Piotto et al. (2002), overplotted with isochrones from Girardi et al. (2000); In the upper panel, 47 Tuc is overplotted with isochrones of $Z=0.004$ and ages 14.0 and 17.7 Gyr, in the lower panel, NGC 6522 is overplotted with isochrones of age 17.7 Gyr and metallicities of $Z=0.001$ and 0.004.

where B = blue HB stars, R = red HB stars, and V = RR Lyrae. Based on a HST CMD from Piotto et al. (2002), we have measured 25 BHB stars, and none in the gap and red HB, assuming

the standard HB gap to be at $0.15 < B-B < 0.45$. Therefore NGC 6522 has an HB parameter of $(B-R)/(B+V+R)=1.0$, a value probably more accurate than the value of 0.71 reported by Terndrup & Walker (1994). This HB morphology together with the $[Fe/H] = -1.0$ metallicity plotted in $[Fe/H]$ vs. HB type shown for example in Lee (1992, Fig. 5) would lead to an age at least 2 Gyr older than typical halo clusters. The same applies to metallicities of $[Fe/H] = -1.1$, and the higher the metallicity the higher the age.

In the following discussion, we argue that these clusters might be the earliest objects in the Galaxy.

The relative ages of 64 Galactic globular clusters, resulting from the corresponding HST Treasury program based on an ACS survey is presented by Marín-Franch et al. (2009). Their Fig. 13 shows an important new result, which is that globular clusters with metallicities $[Fe/H] \geq -1.4$ are found in two types in terms of age. Those of galactocentric radius $R_{GC} < 10$ kpc, are very old. According to Marín-Franch et al. this population is consistent with a galaxy formation scenario of a rapid collapse, and the formation of the old group of clusters within the bulge and halo in a timescale $\lesssim 0.8$ Gyr. Another possibility is that they could also have formed before reionization, in dwarf galaxies that later merged to form the Milky Way. The other group shows younger ages, and are probably formed in satellite dwarf galaxies accreted by the Milky Way.

In Fig. 10 the age and metallicity of NGC 6522 is plotted together with the data on 64 globulars by Marín-Franch et al. (2009). The age of NGC 6522 is assumed to be 2 Gyr older than the mean of globulars as indicated from the Lee (1992) HB type parameter, and the low turn-off. We adopted the metallicity scale of Carretta & Gratton (1997, hereafter CG) rather than the Zinn & West (1984, hereafter ZW) one, for the main reason that CG derived metallicities from clean FeI lines, as in the present analysis. Among the ages reported in Marín-Franch et al. (2009), we adopted those based on the stellar evolution libraries by Dotter et al. (2007) with the option of metallicity compatible with the CG scale. Fig. 10 shows that NGC 6522 would be the oldest cluster in the sample.

We have also plotted in Fig. 10 an estimate of relative age for NGC 6528, that was found to be the most metal-rich cluster in the Galaxy (Zoccali et al. 2004; Ortolani et al. 2007). A com-

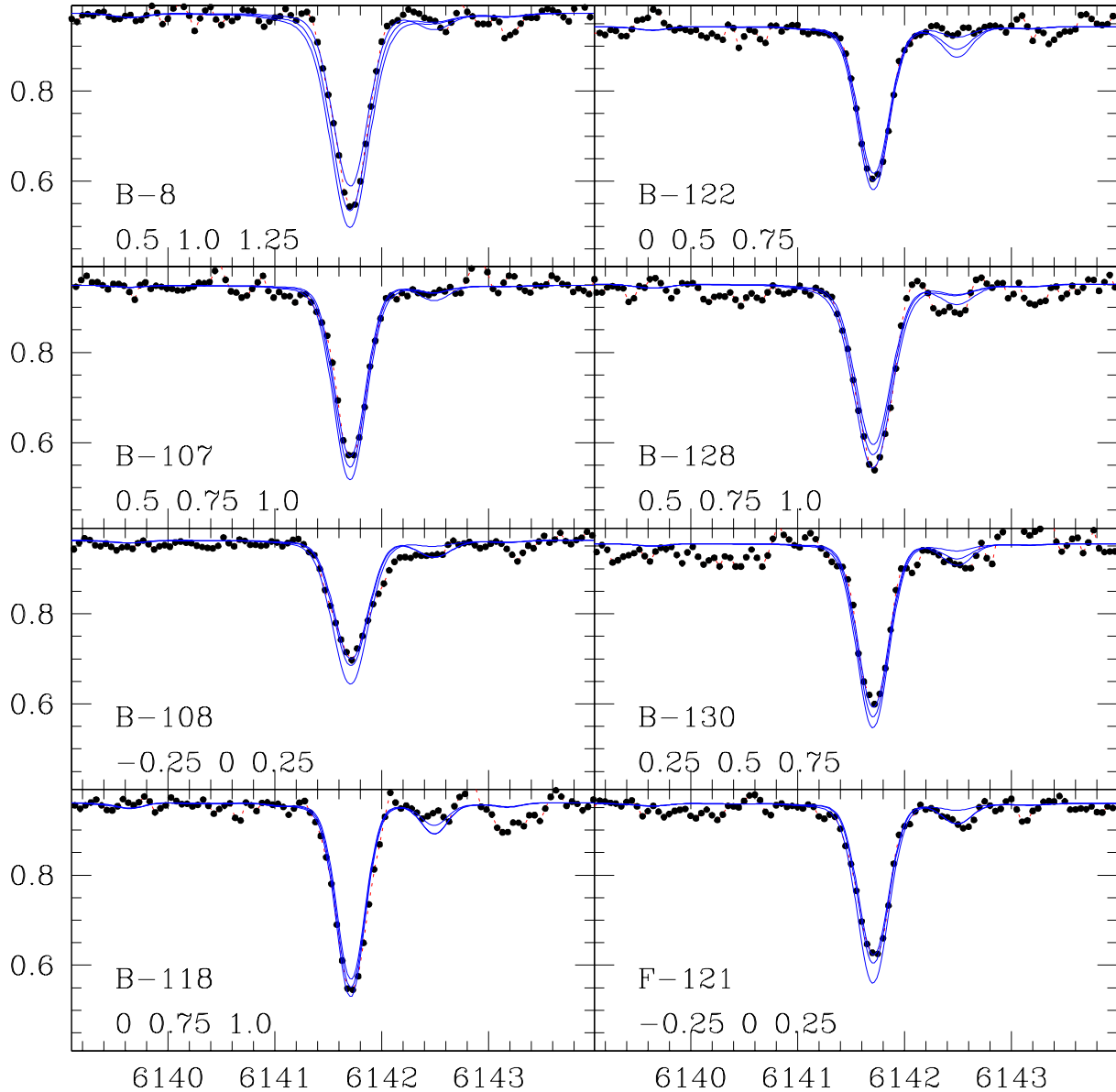


Fig. 7. BaII 6141.727 Å line in the 8 sample stars. Observed spectra are in red and also overplotted with dots. The $[\text{Ba}/\text{Fe}]$ values used in each of the synthetic spectra shown (solid lines) are indicated in the panels.

parison of an ACS CMD for NGC 6528 (Brown et al. 2005) of $[\text{Fe}/\text{H}]=-0.2$ (Zoccali et al. 2004), with that of NGC 6366 of $[\text{Fe}/\text{H}]=-0.44$ in ZW scale, or $[\text{Fe}/\text{H}]=-0.59$ in CG scale (Marín-Franch et al. 2009), and both show $\Delta V(\text{TO-HB})=3.8$, giving a relative age of 1.04 (assuming that the metallicity difference between NGC 6528 and NGC 6366 is small enough to be neglected). We also identify in this Fig. the clusters NGC 6388 and NGC 6441 (Rich et al. 1997), known to have BHBs and high metallicity $[\text{Fe}/\text{H}]\sim-0.6$. These clusters, indicated by full circles in Fig. 10, are different from NGC 6522 in the sense

that NGC 6388 and NGC 6441 have both a blue and a populous red HB.

Another issue concerns the helium abundance: Recio-Blanco et al. (2006) discussed the HB characteristics of 54 BHB globular clusters, and concluded that the blue HB extension depends on metallicity, mass of the cluster (interpreted as self pollution of helium) and age. More parameters could be also involved, as for example concentration and consequent higher collisional probability among member stars. We believe that the hypothesis of a high helium abundance does not apply to NGC 6522: some globular clusters include helium enriched

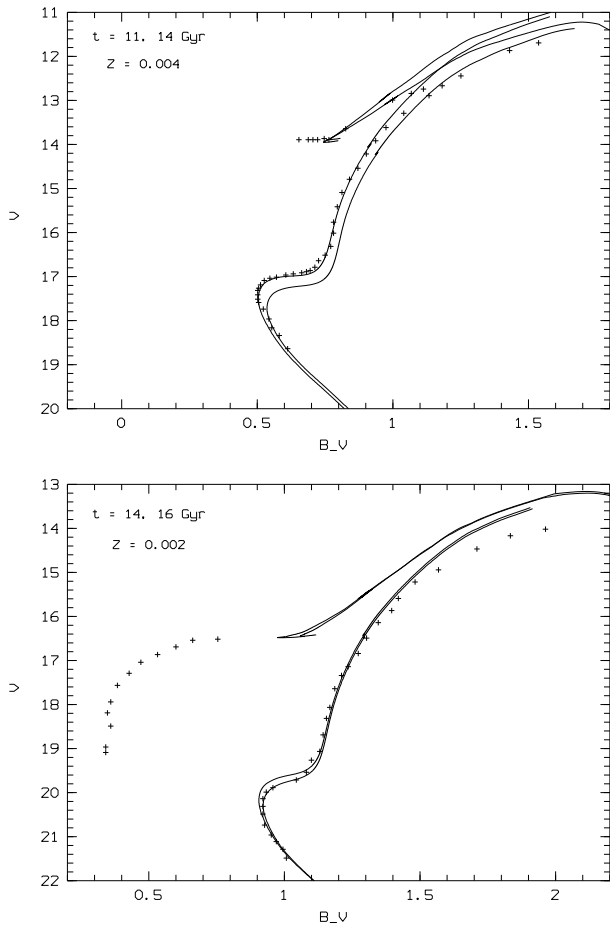


Fig. 9. Mean loci CMDs of 47 Tuc and NGC 6522, based on HST data from Piotto et al. (2002), overplotted with isochrones from Pietrinferni et al. (2004); In the upper panel, 47 Tuc is overplotted with isochrones of $Z=0.004$ and ages 11.0 and 14.0 Gyr, in the lower panel, NGC 6522 is overplotted with isochrones of ages 14.0 and 16.0 Gyr and a metallicity of $Z=0.002$.

sub-populations candidates to explain HB blue extensions (e.g. Piotto et al. 2007, and references therein), however, such helium-enriched populations have been inferred in massive GCs, with mass in excess of $\sim 10^6 M_{\odot}$, involving few of the brightest clusters such as ω Centauri of $M_V = -10.29$ (Harris 1996), which is not the case of NGC 6522 (see also Sect. 1).

7.3. Chemical enrichment scenarios

Our results show enhancements of $[O/Fe]=+0.4$, $[Mg/Fe]=[Si/Fe]\approx+0.25$, and lower $[Ca/Fe]=[Ti/Fe]\approx+0.15$. The odd-Z element Na shows a solar ratio $[Na/Fe]\sim 0.0$. The α -element enhancements in Oxygen, Magnesium and Silicon, together with that of the r-process element Eu $[Eu/Fe]\approx+0.4$ are indicative of a fast early enrichment by Supernovae type II.

The s-elements Ba and La show high ratios $[La/Fe]\approx+0.35$ and $[Ba/Fe]\approx+0.5$. An enhanced Barium abundance is also found in relatively metal-rich globular clusters such as 47 Tucanae (Alves-Brito et al. 2005), M71 (Ramírez & Cohen

Table 6. Classification of inner bulge globular clusters in terms of metallicity and HB morphology (R = Red, B = Blue). References: 1 Ortolani et al. 1997a; 2 Barbuy et al. 1998; 3 Origlia & Rich 2004; 4 Ortolani et al. 1999a; 5 Ortolani et al. 1997b; 6 Barbuy et al. 2006a; 7 Piotto et al. 2002; 8 Rich et al. 1998; 9 Barbuy et al. 2007; 10 Ortolani et al. 2006; 11 Ortolani et al. 1997c; 12 Bica et al. 1994; 13 Ortolani et al. 1997d; 14 Barbuy et al. 1997; 15 Origlia et al. 2005; 16 Ortolani et al. 1999b; 17 Idiart et al. 2002; 18 Lee et al. 2004; 19 Zoccali et al. 2004; 20 Ortolani et al. 2007; 21 Alves-Brito et al. 2006; 22 Ortolani et al. 1996; 23 Origlia et al. 2002; 24 Ortolani et al. 2003; 25 Harris 1996; 26 Barbuy et al. 2006b; 27 Present work; * Note that Davidge (2000) obtained $[Fe/H]=-2.2$ for Djorgovski 1.

cluster	E(B-V)	d_{\odot} (kpc)	[Fe/H]	v_r (km.s ⁻¹)	HB	ref.
Metal-poor						
Terzan 4	1.8	8.3	-1.6	-50	B	1,2,3
Terzan 9	1.95	4.9	-1.0	—	B	4
Moderately metal-poor, BHB						
HP 1	1.21	6.4	-1.0	46	B	5,6
NGC 6522	0.45	7.4	-0.86	-25	B	7,27
NGC 6558	0.38	7.7	-0.97	-197	B	8,9
Al 3	0.36	6	-1.3	—	B	10
Terzan 10	2.4	4.8	-1.0	—	B	2,11
NGC 6540	0.60	3.5	-1.0	—	B	12
Moderately metal-poor, RHB						
Terzan 2	1.6	6.6	-0.5	—	R	2,13
Terzan 6	2.3	5.4	-0.5	—	R	2,14
UKS 1	3.6	10	-0.78	+57	R	11,15
ESO456-SC380.90	5.5	-0.5	—	—	R	2,11
Terzan 1	2.5	5.2	-1.3	114	R	16,17
Palomar 6	1.36	6.40	-1.0	180	R	18
Djorgovski 1	1.70	5.6	-0.4	—	R	2,*
Metal-rich						
NGC 6528	0.46	7.7	-0.1	212	R	19,20
NGC 6553	0.7	5.1	-0.2	-2	R	2,21
Terzan 5	2.39	5.6	-0.3	-93	R	2,3,22
Liller 1	3.7	6	-0.3	+64	R	20,23
Moderately metal-poor, BHB, located in the ring 6° - 12°						
NGC 6325	0.89	6.9	-1.17	29.8	B	7,24,25
NGC 6355	0.75	8.8	-1.3	-176.9	B	7,24,25
NGC 6453	0.61	11.2	-1.53	-83.7	B	7,25
NGC 6626	0.40	5.7	-1.0	17.0	B	25
NGC 6642	0.41	7.2	-1.3	-57.2	B	7,26

2002), and M4 (Ivans et al. 1999). The large abundances of Ba and La, and their large star-to-star variations are illustrated in Fig. 7, showing the BaII 6141.727 Å in the 8 sample stars. The high La and Ba abundances are consistent with each other, but the $[Ba/Eu]=+0.1$ ratio, that could give a measure of the s- to r-process nucleosynthesis, is too high, and clearly the La and Ba excesses cannot be attributed to the r-process. The s-elements excesses could be due to an s-process enrichment of the primordial matter from which the cluster formed, or else s-process the occurred in nearby Asymptotic Giant Branch (AGB) stars during He shell flash episodes, and the ejected material would

be accreted by the sample stars during their formation process. This latter explanation would also account for the large spread in the Ba abundances.

The star-to-star variation of the r-process element Eu are more difficult to explain, since r-elements are only produced in supernovae events. The only explanation would be a primordial enrichment by different supernovae, and no gas mixing prior to the formation of the sample stars. The spectral region of the EuII 6645.127 Å line is however rather noisy, and we prefer not to draw conclusions on these Eu abundance variations.

Finally, Table 9 and Fig. 11 show a comparison of abundance ratios in NGC 6522, with a) results by Origlia & Rich (2004) for the metal-poor cluster Terzan 4 ($[\text{Fe}/\text{H}] = -1.6$), also located in the inner bulge for which significant enhancements of α -elements were found, and UKS 1, a moderate metallicity cluster ($[\text{Fe}/\text{H}] = -0.78$) with moderate enhancements, b) the clusters HP 1 and NGC 6558. HP 1 and NGC 6558, similarly to NGC 6522, show a peculiar pattern and might be revealing characteristics of the early bulge chemical enrichment. It would be of great interest to have further analyses of individual stars in the three clusters HP-1, NGC 6558 and NGC 6522 and other metal-poor bulge globular clusters.

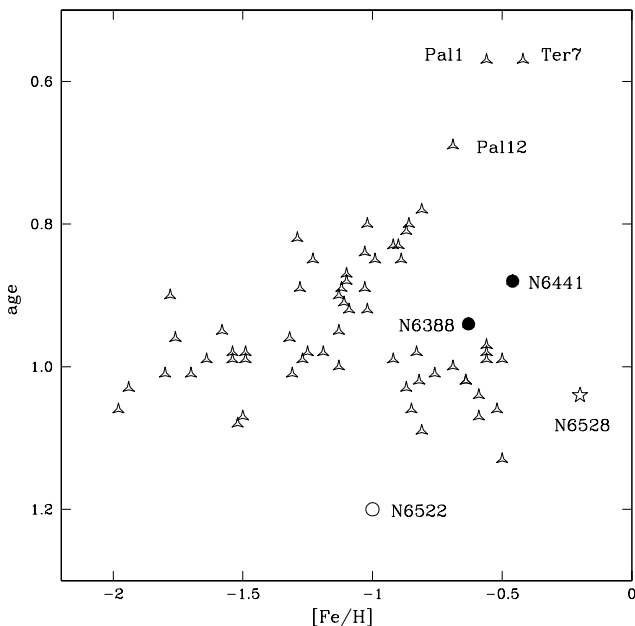


Fig. 10. Age vs. metallicities, given in the CG metallicity scale, of the 64 globular clusters from Marín-Franch et al. (2009), and the location of NGC 6522 in the plot, showing it to be the oldest cluster of this sample (open circle). The most metal-rich bulge cluster NGC 6528 ($[\text{Fe}/\text{H}] = -0.2$) is identified with an open star. The metal-rich $[\text{Fe}/\text{H}] = -0.6$ clusters that have an extended blue HB and a red HB, NGC 6388 and NGC 6441, are indicated by full circles. Some of the youngest clusters Pal 1, Pal 12 and Ter 7 are also identified.

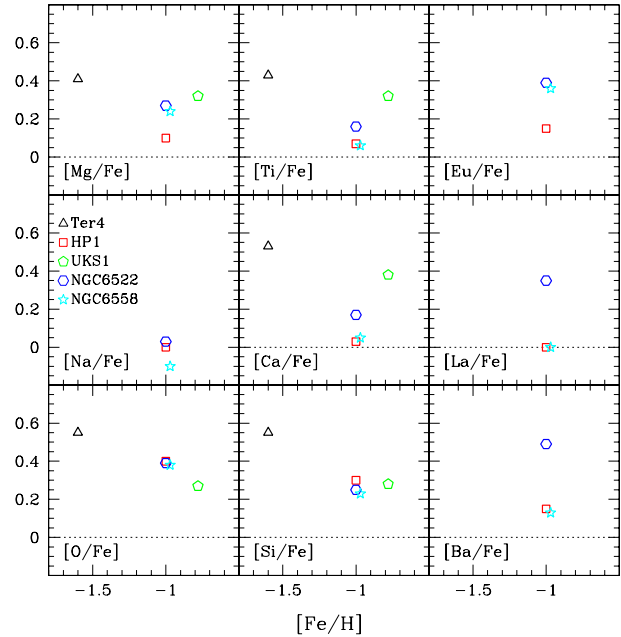


Fig. 11. Abundance pattern of NGC 6522 compared to other metal-poor globular clusters located in the Galactic bulge.

8. Conclusions

Lee (1992) pointed out that RR Lyrae in the Galactic bulge have a peak metallicity of $[\text{Fe}/\text{H}] \approx -1.0$. This population should be older than the halo, because being more metal-rich these stars should be more massive, and expected to populate the red HB, whereas given that they populate the RR Lyrae gap, then a lower mass is required for them, consequently implying older ages.

The metallicity of $[\text{Fe}/\text{H}] \approx -1.0$ was derived for NGC 6522, based on high resolution spectra, similarly to results found for HP 1 and NGC 6558. This relatively high metallicity was unexpected given that in the literature, the metallicity values quoted are in the range $[\text{Fe}/\text{H}] = -1.3$ to -1.5 along the last decades (Table 1). Besides, this moderate metallicity combined to a blue horizontal branch, indicates an old age for these clusters, similarly to the RR Lyrae results by Lee (1992).

The bulge metallicity distribution, based on FLAMES+GIRAFFE high resolution spectroscopy of 800 stars by Zoccali et al. (2008), shows that the metallicity of NGC 6522 corresponds to the lower end of the distribution.

Abundance ratios in NGC 6522 show enhancements of the α -elements O, Mg and Si, whereas Ti and Ca enhancements are shallower. This pattern is shared by the similar clusters HP 1 and NGC 6558. The shallow Ca and Ti abundances in these three clusters differs from somewhat higher values in halo clusters, that is found as well in the abundances of the central metal-poor cluster Terzan 4, as shown in Fig. 11. The Eu excesses are compatible among the three clusters and as well with halo clusters. The high abundances of the s-elements La and Ba and not found in HP 1 and NGC 6558. These high values and the star-to-star variation are puzzling, and might point to internal contamination from nearby AGB stars.

In the present paper other possible members of this class of clusters showing moderate metallicity around $[Fe/H] \approx -1.0$ and blue Horizontal Branch are reported, and it would be of great interest to study them by means of high resolution spectroscopy.

Acknowledgements. BB and EB acknowledge grants from CNPq and Fapesp. DM acknowledges support from the FONDAP Center for Astrophysics 15010003, the BASAL Center for Astrophysics and Associated Technologies PFB06, and FONDECYT Project 1090213. SO acknowledges the Italian Ministero dell'Università e della Ricerca Scientifica e Tecnologica (MURST), Italy. This publication makes use of data products from the Two Micron All Sky Survey, which is a joint project of the University of Massachusetts and the Infrared Processing and Analysis Center/California Institute of Technology, funded by the National Aeronautics and Space Administration and the National Science Foundation.

References

- Allende Prieto, C., Lambert, D.L., Asplund, M. 2001, ApJ, 556, L63
 Alves-Brito, A., Barbuy, B., Ortolani, S., et al. 2005, A&A, 435, 657
 Alves-Brito, A., Barbuy, B., Zoccali, M., et al. 2006, A&A, 460, 269
 Alonso, A., Arribas, S., Martínez-Roger, C. 1998, A&AS, 131, 209
 Alonso, A., Arribas, S., Martínez-Roger, C. 1999, A&AS, 140, 261
 Armandroff, T. 1989, AJ, 97, 375
 Baade, W. 1946, PASP, 58, 249
 Barbuy, B., Ortolani, S., Bica, E. 1994, A&A, 285, 871
 Barbuy, B., Ortolani, S., Bica, E. 1997, A&AS, 122, 483
 Barbuy, B., Bica, E., Ortolani, S. 1998, A&A, 333, 117
 Barbuy, B., Perrin, M.-N., Katz, D. et al. 2003, A&A, 404, 661
 Barbuy, B., Zoccali, M., Ortolani, S., et al. 2006a, A&A, 449, 349
 Barbuy, B., Bica, E., Ortolani, S., Bonatto, C. 2006b, A&A, 449, 1019
 Barbuy, B., Zoccali, M., Ortolani, S., et al. 2007, AJ, 134, 1613
 Barklem, P.S., Anstee, S.D., O'Mara, B.J. 1998, PASA, 15, 336
 Barklem, P.S., Piskunov, N.E., O'Mara, B. J. 2000, A&AS, 142, 467
 Bessell, M.S. 1979, PASP, 91, 589
 Bica, E., Ortolani, S., Barbuy, B. 1994, A&A, 283, 67
 Bica, E., Bonatto, C., Barbuy, B., Ortolani, S. 2006, A&A, 450, 105
 Biémont, E., Baudoux, M., Kurúcz, R.L., Ansbacher, W., Pinnington, A.E., 1991, A&A, 249, 539
 Blanco, V.M., Blanco, B.M. 1984, PASP, 96, 603
 Brown, T.A., Ferguson, H.C., Smith, E. et al. 2005, AJ, 130, 1693
 Carpenter, J.M. 2001, AJ, 121, 2851
 Carretta, E., Gratton, R.G. 1997, A&AS, 121, 95
 Clement, C.M., Muzzin, A., Dufton, Q., et al. 2001, AJ, 122, 2587
 Coelho, P., Barbuy, B., Meléndez, J., Schiavon, R.P., Castilho, B.V. 2005, A&A, 443, 735
 Davidge, T. 2000, ApJS, 126, 105
 Dean, J.F., Warpen, P.R., Cousins, A.J.: 1978, MNRAS, 183, 569
 Diemand, J., Madau, P., Moore, B. 2005, MNRAS, 364, 367
 Dotter, A., Chaboyer, B., Jevremović, D., et al. 2007, AJ, 134, 376
 Fuhr, J.R., Wiese, W.L. 2006, J. Phys. Chem. Ref. Data, 35, 1669
 Hazen, M.L. 1996, AJ, 111, 1184
 Grevesse, N., Sauval, J. 1998, Space Sci. Rev., 85, 161 ed. S. S. Holt & G. Sonneborn (San Francisco: ASP), 117
 Gustafsson, B., Edvardsson, B., Eriksson, K., Jorgensen, U.G., Nordlund, Å., Plez, B. 2008, A&A, 486, 951
 Harris, W.E. 1996, AJ, 112, 1487
 Hill, V., Plez, B., Cayrel, R. et al. 2002, A&A, 387, 560
 Idiart, T., Barbuy, B., Perrin, M.-N., et al. 2002, A&A, 381, 472
 Ivans, I., Sneden, C., Kraft, R.P. et al. 1999, AJ, 118, 1273
 Kraft, R.P., Ivans, I.I. 2003, PASP, 115, 143
 Koch, A., McWilliam, A. 2008, AJ, 135, 1551
 Lawler, J.E., Wickliffe, M.E., den Hartog, E., Sneden, C. 2001a, ApJ, 563, 1075
 Lawler, J.E., Bonvallet, G., Sneden, C. 2001b, ApJ, 556, 452
 Lecureur, A., Hill, V., Zoccali, M., et al. 2007, A&A, 465, 799
 Lee, Y.-W. 1992, AJ, 104, 1780
 Lee, Y.-W., Demarque, P., Zinn, R. 1994, ApJ, 423, 248
 Lee, J.-W., Carney, B.W., Balachandran, S.C. 2004, AJ, 128, 2388
 Lee, Y.-K., Gim, H.S., Casetti-Dinescu, D.I. 2007, ApJ, 661, L49
 Marín-Franch, A., Aparicio, A., Piotto, G., Rosenberg, A., Chaboyer, B., et al. 2009, ApJ, 694, 1498
 McWilliam, A. 1998, AJ, 115, 1640
 Meléndez, J., Barbuy, B., 2009, A&A, 497, 611
 Minniti, D., Olszewski, E.W., Rieke, M. 1995, AJ, 110, 1686
 Moore, B., Diemand, J., Madau, P., Zemp, M., Stadel, J. 2006, MNRAS, 368, 563
 Origlia, L., Rich, R.M. 2004, AJ, 127, 3422
 Origlia, L., Valenti, E., Rich, R.M., Ferraro, F.R. 2005, MNRAS, 363, 897
 Ortolani, S., Barbuy, B., Bica, E. 1996, A&A, 308, 733
 Ortolani, S., Barbuy, B., Bica, E. 1997a, A&A, 319, 850
 Ortolani, S., Bica, E., Barbuy, B. 1997b, MNRAS, 284, 692
 Ortolani, S., Bica, E., Barbuy, B. 1997c, A&AS, 126, 319
 Ortolani, S., Bica, E., Barbuy, B. 1997d, A&A, 326, 614
 Ortolani, S., Bica, E., Barbuy, B. 1999a, A&AS, 138, 267
 Ortolani, S., Barbuy, B., Bica, E., et al. 1999b, A&A, 350, 840
 Ortolani, S., Bica, E., Barbuy, B. 2003, A&A, 402, 565
 Ortolani, S., Bica, E., Barbuy, B. 2006, ApJ, 646, L115
 Ortolani, S., Barbuy, B., Bica, E., Zoccali, M., Renzini, A. 2007, A&A, 470, 1043
 Pietrinferni, A., Cassisi, S., Salaris, M., Castelli, F. 2004, ApJ, 612, 168
 Piotto, G., Bedin, L., Anderson, J. et al. 2007, ApJ, 661, L53
 Piotto, G., King, I.R., Djorgovski, S.G., et al. 2002, A&A, 391, 945
 Ramírez, S.V., Cohen, J.G. 2002, AJ, 123, 3277
 Recio Blanco, A., Aparicio, A., Piotto, G., de Angeli, F., Djorgovski, S.G. 2006, A&A, 452, 875
 Rich, R.M., Sosin, C., Djorgovski, S.G., et al. 1997, ApJ, 484, L25
 Rich, R.M., Ortolani, S., Bica, E., Barbuy, B. 1998, AJ, 116, 1295
 Rieke, G.H., Lebofsky, M.J., 1985, ApJ, 288, 618
 Rutledge, G.A., Hesser, J.E., Stetson, P.B. et al. 1997a, PASP, 109, 883
 Rutledge, G.A., Hesser, J.E., Stetson, P.B. 1997b, PASP, 109, 907
 Rutten, R.J. 1978, SoPh, 56, 237
 Skrutskie, M., Cutri, R.M., Stiening, R., et al. 2006, AJ, 131, 1163
 Spergel, D.N., Verde, L., Peiris, H.V. et al. 2003, ApJS, 148, 175
 Stetson, P.B., Pancino, E. 2008, PASP, 120, 1332
 Suntzeff, N.B., Kinman, T.D., Kraft, R.P. 1991, ApJ, 367, 528
 Terzan A. 1964a, Haute Prov. Publ., 7, 2
 Terzan A. 1964b, Haute Prov. Publ., 7, 3
 Terzan A. 1965, Haute Prov. Publ., 8, 11
 Terzan A. 1966, Haute Prov. Publ., 8, 12
 Trager, S.C., King, I.R., Djorgovski, S. 1995, AJ, 109, 218
 Terndrup, D.M., Walker, A.R., 1994, AJ, 107, 1786
 Terndrup, D.M., Popowski, P., Gould, A., Rich, R.M., Sadler, E.M. 1998, AJ, 115, 1476
 Walker, A.R., Mack, P. 1986, MNRAS, 220, 69
 Walker, A.R., Terndrup, D.M. 1991, ApJ, 378, 119
 Yong, D., Karakas, A.I., Lambert, D.L., Chieffi, A., Limongi, M. 2008, ApJ, 689, 1031
 Zinn, R., West, M.J. 1984, ApJS, 55, 45
 Zinn, R. 1985, ApJ, 293, 424
 Zoccali, M., Barbuy, B., Hill, V., et al. 2004, A&A, 423, 507
 Zoccali, M., Lecureur, A., Barbuy, B. et al. 2006, A&A, 457, L1
 Zoccali, M., Lecureur, A., Hill, V. et al. 2008, A&A, 486, 177

Table 7. Abundance ratios derived and atomic parameters adopted. Column 5 reports the log gf adopted as described in Barbuy et al. (2007). For the heavy elements BaII, LaII and EuII, hyperfine structure was taken into account, and the log gf values reported correspond to the equivalent total log gf, adopted from a Hill et al. (2002), b Rutten (1978), c Lawler et al. (2001b).

Species	λ (Å)	χ_{ex} (eV)	C_6 (cm^6s^{-1})	loggf	[X/Fe]							
					B-8	B-107	B-108	B118	B-122	B-128	B-130	F-121
OI	6300.311	0.00	0.30E-31	-9.716	+0.3:	—	—	—	—	—	+0.5:	+0.5:
OI	6363.79	0.00	0.30E-31	-10.25	+0.2:	+0.5:	+0.7:	+0.3:	+0.7:	—	—	+0.5:
NaI	6154.230	2.10	0.90E-31	-1.56	+0.3	-0.3:	0.0	+0.1	+0.1	+0.1	+0.1	-0.1
NaI	6160.753	2.10	0.30E-31	-1.26	+0.4	-0.3:	-0.2	+0.1	+0.2	+0.1	+0.2	-0.1
MgI	6318.720	5.11	0.30E-31	-2.10	+0.1:	+0.20	+0.4:	+0.2	+0.2	+0.2	+0.4	+0.4
MgI	6319.242	5.11	0.30E-31	-2.36	+0.1:	—	+0.2:	0.0	+0.2	+0.2	+0.4	+0.4
MgI	6319.490	5.11	0.30E-31	-2.80	+0.1:	+0.20	+0.4:	+0.2	+0.2	+0.4	+0.4	+0.4
MgI	6765.450	5.75	0.30E-31	-1.94	—	+0.40:	—	—	—	+0.2:	+0.4:	+0.4:
SiI	6142.494	5.62	0.30E-31	-1.50	+0.2	+0.2	+0.4	+0.2	0.0	+0.2	+0.4	+0.2
SiI	6145.020	5.61	0.30E-31	-1.45	+0.4	+0.2	+0.2	+0.2	+0.2	+0.2	—	+0.2
SiI	6155.142	5.62	0.30E-30	-0.85	+0.2	+0.1	0.0	+0.2	-0.1	+0.2	+0.3	+0.2
SiI	6237.328	5.61	0.30E-30	-1.01	+0.4	+0.2	+0.2	+0.3	+0.2	+0.3	+0.4	+0.4
SiI	6243.823	5.61	0.30E-32	-1.30	+0.4	+0.2	+0.2	+0.4	+0.3	+0.4	+0.4	+0.4
SiI	6414.987	5.87	0.30E-30	-1.13	+0.4:	+0.2	+0.2	+0.4	+0.2	+0.2	+0.2	+0.2
SiI	6721.844	5.86	0.90E-30	-1.17	+0.4	+0.3	+0.2	+0.3	—	+0.2:	+0.4:	—
CaI	6156.030	2.52	4.0E-31	-2.39	—	+0.3	+0.1	0.0	0.0	+0.3	—	0.0:
CaI	6161.295	2.51	4.0E-31	-1.02	+0.2	0.0	+0.3	0.0	+0.3	+0.2	+0.3	+0.3
CaI	6162.167	1.89	3.0E-31	-0.09	0.0	+0.2	0.0	+0.2	0.0	0.0	+0.1	+0.3
CaI	6166.440	2.52	3.97E-31	-0.90	0.0	0.0	+0.2	+0.2	+0.3	0.0	+0.3	+0.3
CaI	6169.044	2.52	3.97E-31	-0.54	+0.3	+0.1	+0.1	+0.2	+0.3	+0.3	+0.1	+0.3
CaI	6169.564	2.52	4.0E-31	-0.27	+0.1	+0.2	+0.1	+0.3	+0.3	+0.3	+0.2	+0.3
CaI	6439.080	2.52	3.4E-32	+0.3	0.0	+0.3	+0.3	+0.3	+0.3	+0.3	+0.3	0.0
CaI	6455.605	2.52	3.39E-32	-1.35	+0.3	0.0	+0.3	+0.3	+0.3	-0.1	+0.4:	+0.3
CaI	6464.679	2.52	3.4E-32	-2.10	+0.3	0.0	+0.3	+0.3	+0.3	+0.3:	—	+0.3
CaI	6471.668	2.52	3.39E-32	-0.59	+0.3	0.0	+0.3	+0.3	+0.3	+0.3	+0.3	+0.3
CaI	6493.788	2.52	3.37E-32	0.0	+0.1	-0.3	0.0	+0.2	0.0	0.0	+0.1	-0.2
CaI	6499.654	2.52	3.37E-32	-0.85	+0.2	-0.3	+0.2	0.0	0.0	0.0	+0.1	-0.1
CaI	6572.779	0.00	1.75E-32	-4.32	+0.1	0.0	+0.3	+0.3	+0.2	0.0	+0.2	0.0
CaI	6717.687	2.71	4.1E-31	-0.61	0.0	0.0	0.0	+0.3	+0.3	+0.3	+0.3	+0.1
TiI	6126.224	1.07	1.37E-32	-1.43	+0.2	+0.2	+0.2	0.0	+0.1	+0.1	+0.2	0.0
TiI	6258.110	1.44	3.17E-32	-0.36	0.0	0.0	+0.2	0.0	+0.2	+0.2	0.0	+0.1
TiI	6261.106	1.43	4.68E-32	-0.48	0.0	0.0	0.0	0.0	+0.3	0.0	0.0	+0.2
TiI	6303.767	1.44	3.12E-32	-1.57	0.0:	0.0	—	+0.2	+0.2:	+0.2:	—	—
TiI	6336.113	1.44	1.86E-32	-1.74	—	—	+0.2:	+0.3	+0.3	0.0:	—	+0.3:
TiI	6554.238	1.44	1.81E-32	-1.22	+0.2	+0.2	+0.2	0.0	+0.2	+0.2	0.0	+0.2
TiI	6556.077	1.46	1.81E-32	-1.07	0.0	+0.2	+0.3	0.0	0.0	+0.2	+0.4	+0.2
TiI	6599.113	0.90	1.96E-32	-2.09	+0.2:	+0.3	+0.2:	+0.3	+0.2	+0.2:	+0.4:	+0.1
TiI	6743.127	0.90	0.30E-31	-1.73	0.0	+0.1	+0.2	-0.2	0.0	0.0	+0.2	+0.2
TiII	6491.580	2.06	0.30E-31	-2.10	+0.2	+0.3	+0.3	+0.3	+0.3	+0.3	+0.3	+0.1
TiII	6559.576	2.05	0.30E-31	-2.35	+0.3	0.0	+0.3	+0.3	+0.3	+0.3	+0.3	+0.2
TiII	6606.970	2.06	0.30E-31	-2.85	+0.2	+0.2:	+0.2	—	—	+0.3:	+0.3	+0.2
BaII	6141.727	0.70		-0.07 ^a	+1.0	+0.5	-0.1	+0.75	+0.5	+1.0	+0.25	-0.25
BaII	6496.908	0.60		-0.38 ^b	+0.9	+0.5	+0.15	+1.2	+0.75	+0.75	+0.25	-0.25
LaII	6390.480	0.32		-1.41 ^c	+0.5	+0.50	+0.3	+0.5	+0.3:	—	—	0.0:
EuII	6645.127	1.38		0.12 ^a	+0.5	0.0:	+0.5:	+0.5	+0.3:	0.0:	+0.8	+0.5

Table 8. Final abundances for each sample star, and mean results and corresponding internal errors.

Element	B-8	B-107	B-108	B-118	B-122	B-128	B-130	F-121	Mean
[O/Fe]	+0.25:	+0.5:	+0.7:	+0.3:	+0.7:	—	+0.5:	+0.5:	+0.39:±0.3
[Na/Fe]	+0.35	-0.30	-0.15	+0.10	+0.15	+0.10	+0.15	-0.10	+0.03±0.3
[Mg/Fe]	+0.10	+0.27	+0.33	+0.20	+0.20	+0.25	+0.40	+0.40	+0.27±0.15
[Si/Fe]	+0.34	+0.20	+0.20	+0.29	+0.13	+0.24	+0.35	+0.27	+0.25±0.10
[Ca/Fe]	+0.15	+0.04	+0.18	+0.21	+0.21	+0.16	+0.23	+0.16	+0.17±0.06
[Ti/Fe]	+0.12	+0.14	+0.21	+0.11	+0.19	+0.17	+0.21	+0.16	+0.16±0.04
[Eu/Fe]	+0.50	0.00	+0.50	+0.50	+0.30	0.00	+0.80	+0.50	+0.39±0.4
[Ba/Fe]	+0.95	+0.50	0.0	+1.00	+0.60	+0.90	+0.25	-0.25	+0.49±0.4
[La/Fe]	+0.50	+0.50	+0.30	+0.50	+0.30	—	—	0.00	+0.35±0.2

Table 9. Final abundance ratios $[X/Fe]$ of NGC 6522, compared with those of the metal-poor bulge clusters HP 1 (Barbuy et al. 2006), NGC 6558 (Barbuy et al. 2007), UKS 1 (Origlia et al. 2005) and Terzan 4 (Origlia et al. 2004). In the 2nd column the solar abundances adopted are reported.

Species	$\epsilon(X)_{\odot}$	NGC 6522	NGC 6558	HP 1	UKS 1	Terzan 4
[Fe/H]	7.50	-1.00	-0.97	-0.99	-0.78	-1.60
[OI/Fe]	8.77	+0.39	+0.38	+0.40	+0.27	+0.55
[NaI/Fe]	6.33	+0.03	-0.09	+0.00	—	—
[MgI/Fe]	7.58	+0.27	+0.24	+0.10	+0.32	+0.41
[SiI/Fe]	7.55	+0.25	+0.23	+0.30	+0.28	+0.55
[CaI/Fe]	6.36	+0.17	+0.05	+0.03	+0.38	+0.53
[TiI,II/Fe]	5.02	+0.16	+0.06	+0.08	+0.32	+0.43
[BaII/Fe]	2.13	+0.49	+0.13	+0.15	—	—
[LaII/Fe]	1.22	+0.35	0.00	+0.00	—	—
[EuII/Fe]	0.51	+0.39	+0.36	+0.15	—	—

Online Material

Table 1. Fe I and FeII line list, wavelength, excitation potential, damping constant, gf-values and equivalent widths. The oscillator strengths used in this paper and in Barbuy et al. (2007) are given in column 6, and compared to those given in Fuhr & Wiese (2006) in column 5. Equivalent widths were measured using DAOSPEC. For B-108 and B-134 the lines were checked with IRAF, and only very clean lines were kept.

Species	λ (Å)	χ_{ex} (eV)	C_6 cm^6s^{-1}	$\log gf$ FW06	$\log gf$ present	B-8	B-107	B-108	B-118	B-122	B-128	B-130	B-134	F-121
FeII	6149.26	3.89	0.34E-32	-2.84	-2.69	18	31	22	23	25	31	32	40	20
FeII	6247.56	3.89	0.33E-32	-2.43	-1.98	43	51	25	43	42	44	43	57	43
FeII	6432.68	2.89	0.24E-32	-3.57	-3.57	35	42	28	29	33	38	38	38	30
FeII	6456.39	3.90	0.32E-32	-2.19	-2.05	60	76	49	62	53	51	53	85	47
FeII	6516.08	2.89	0.25E-32	-3.37	-3.31	52	53	34	40	44	44	43	60	49
FeI	6151.62	2.18	0.81E-32	same	-3.299	73	44	52	74	59	68	52	27	56
FeI	6159.38	4.61	0.13E-30	absent	-1.97	24	—	—	—	—	—	13	—	—
FeI	6165.36	4.14	0.77E-31	-1.474	-1.549	32	23	—	37	—	29	25	7	25
FeI	6173.34	2.22	0.84E-32	-2.880	-2.879	95	67	62	99	88	92	78	—	75
FeI	6180.20	2.73	0.13E-31	-2.650	-2.784	78	44	50	68	58	70	60	12	54
FeI	6187.99	3.94	0.30E-30	-1.670	-1.718	40	22	21	42	27	34	31	19	26
FeI	6200.31	2.61	0.15E-31	same	-2.437	83	64	66	81	73	81	76	11	75
FeI	6213.43	2.22	0.30E-31	-2.48	-2.646	109	87	78	99	96	98	91	35	87
FeI	6220.78	3.88	0.13E-30	absent	-2.46	22	11	—	16	—	—	—	—	12
FeI	6226.74	3.88	0.13E-30	absent	-2.202	23	16	—	15	16	17	15	17	17
FeI	6240.65	2.22	0.10E-31	-3.17	-3.388	71	86	45	68	57	73	50	—	56
FeI	6246.32	3.60	0.12E-30	-0.877	-0.956	102	86	73	102	95	110	100	64	99
FeI	6252.56	2.40	0.12E-31	same	-1.687	140	117	103	126	116	118	119	82	119
FeI	6254.25	2.28	0.13E-31	-2.426	-2.480	115	103	87	127	108	116	106	52	106
FeI	6270.23	2.86	0.15E-31	-2.61	-2.711	73	36	51	67	60	72	62	21	56
FeI	6271.28	3.32	0.89E-31	-2.703	-2.957	17	9	18	21	—	12	—	13	14
FeI	6297.79	2.22	0.82E-32	same	-2.740	97	58	63	88	75	90	72	25	71
FeI	6301.50	3.65	0.23E-31	-0.718	-0.720	100	90	67	89	84	86	90	—	86
FeI	6302.50	3.69	0.23E-31	absent	-0.91	91	75	66	70	72	88	79	37	73
FeI	6311.50	2.83	0.14E-31	-3.141	-3.224	46	28	38	45	43	46	44	32	25
FeI	6315.31	4.14	0.30E-31	-1.232	-1.230	55	42	33	52	42	48	33	—	43
FeI	6315.81	4.08	0.66E-31	-1.660	-1.712	38	30	30	41	42	39	30	—	23
FeI	6322.69	2.59	0.14E-31	same	-2.426	92	69	59	91	77	89	70	28	78
FeI	6335.33	2.20	0.80E-32	-2.177	-2.229	114	106	90	109	110	120	103	—	99
FeI	6336.82	3.69	0.13E-30	-0.856	-1.053	101	77	70	90	80	—	69	36	84
FeI	6344.15	2.43	0.12E-31	-2.923	-2.922	93	56	55	78	75	84	65	29	70
FeI	6355.03	2.84	0.30E-31	-2.291	-2.40	97	35	58	89	80	94	70	24	74
FeI	6392.54	2.28	0.11E-31	absent	-4.03	42	—	—	31	18	24	31	—	21
FeI	6393.60	2.43	0.12E-31	-1.58	-1.615	183	136	107	144	123	152	143	—	107
FeI	6419.95	4.73	0.15E-30	-0.27	-0.250	64	41	47	66	53	62	53	28	52
FeI	6430.85	2.18	0.77E-32	-2.006	-2.005	133	112	116	133	121	133	124	74	97
FeI	6475.62	2.56	0.15E-31	same	-2.94	77	42	57	77	57	64	61	17	44
FeI	6481.87	2.28	0.11E-31	same	-2.984	87	58	64	81	72	78	74	25	55
FeI	6498.94	0.96	0.49E-32	-4.687	-4.699	87	44	74	71	68	73	70	15	51
FeI	6518.37	2.83	0.13E-31	-2.30	-2.748	61	46	45	50	60	61	48	19	50
FeI	6533.93	4.56	0.16E-30	-1.43	-1.453	20	19	—	—	25	—	25	—	19
FeI	6569.22	4.73	0.13E-30	-0.45	-0.422	59	38	49	62	52	69	62	—	45
FeI	6574.23	0.99	0.56E-32	-5.004	-5.042	63	18	41	64	49	50	45	—	51
FeI	6575.02	2.59	0.14E-31	-2.71	-2.824	85	47	57	78	69	79	64	—	62
FeI	6591.31	4.59	0.12E-30	absent	-2.06	—	—	—	—	—	9	—	—	—
FeI	6593.87	2.43	0.12E-31	same	-2.422	105	86	86	115	98	105	87	—	80
FeI	6597.56	4.80	0.15E-30	-1.05	-1.061	33	13	21	28	31	34	17	19	25
FeI	6608.03	2.28	0.10E-31	absent	-4.038	16	7	—	14	25	15	13	6	16
FeI	6678.00	2.69	0.30E-31	absent	-1.420	147	118	—	150	139	148	134	—	128
FeI	6703.57	2.76	0.12E-31	-3.06	-3.15	51	35	28	40	37	54	19	19	33

B. Barbuy et al.: Abundances in 8 giants of NGC 6522, *Online Material p 4*

FeI	6705.11	4.61	0.30E-31	absent	-1.060	34	—	—	29	12	40	26	—	22
FeI	6710.32	1.48	0.64E-32	absent	-4.874	46	14	—	49	31	46	32	—	34
FeI	6713.75	4.80	0.16E-30	absent	-1.602	—	—	—	16	—	—	5	—	7
FeI	6715.38	4.59	0.11E-30	absent	-1.638	32	17	—	14	12	27	18	—	18
FeI	6716.24	4.56	0.79E-32	absent	-1.927	15	11	—	—	8	31	10	—	11
FeI	6725.36	4.10	0.15E-30	absent	-2.300	—	—	—	9	10	5	20	—	16
FeI	6726.67	4.59	0.30E-31	absent	-1.090	22	—	27	24	34	18	32	—	24
FeI	6733.15	4.64	0.11E-30	absent	-1.576	25	22	—	30	27	31	18	—	23
FeI	6739.52	1.56	0.67E-32	-4.79	-4.941	33	—	—	26	36	25	25	—	30
FeI	6752.71	4.64	0.11E-30	-1.204	-1.366	22	27	—	23	28	23	6	—	21
FeI	6810.26	4.60	0.14E-30	-0.986	-1.108	31	11	—	44	25	35	32	—	17
FeI	6820.37	4.64	0.16E-30	-1.29	-1.311	36	12	—	45	23	30	14	—	24
FeI	6837.02	4.59	0.78E-32	-1.687	-1.800	13	—	—	22	—	—	24	—	14
FeI	6839.83	2.56	0.13E-31	-3.35	-3.451	49	24	—	37	32	47	35	—	27
FeI	6841.34	4.61	0.10E-30	-0.78	-0.752	49	27	—	56	53	55	17	—	39
FeI	6842.69	4.64	0.15E-30	-1.29	-1.315	20	11	—	23	44	38	—	—	13
FeI	6843.66	4.55	0.94E-31	-0.89	-0.928	50	23	—	47	53	64	32	—	42
FeI	6851.63	1.60	0.73E-32	absent	-5.307	26	21	—	18	20	30	8	—	—
FeI	6855.71	4.39	0.10E-30	absent	-1.819	33	35	—	45	17	28	25	—	28
FeI	6857.25	4.08	0.53E-31	absent	-2.156	15	17	—	14	13	24	8	—	21
FeI	6858.15	4.61	0.10E-30	-0.93	-1.055	39	30	—	30	35	41	13	—	24